Available online at www.sciencedirect.com
ScienceDirect
Trans. Nonferrous Met. Soc. China 24(2014) 2896−2903
Transactions of Nonferrous Metals Society of China
www.tnmsc.cn

Preparation and sensing performance of petal-like RuO_2 modified ZnO nanosheets via a facile solvothermal and calcination method

Yan LI, Guo-zhu LI, Yun-ling ZOU, Qiong WANG, Qing-jun ZHOU, Xiao-xue LIAN

Institute of Aerochemistry, College of Science, Civil Aviation University of China, Tianjin 300300, China

Received 29 September 2013; accepted 19 May 2014

Abstract: Petal-like ZnO nanosheets were synthesized with zinc nitrate hexahydrate and sodium hydroxide as starting materials in ammonia and ethanol mixture solution. RuO_2 modified ZnO nanosheets were also prepared by a calcination route. The as-prepared products were characterized by X-ray powder diffraction and field emission scanning electron microscopy, and its specific BET surface area was calculated by nitrogen adsorption method. The sensitivity, response and recovery speed were examined. The results show that RuO_2 modified petal-like ZnO based sensor exhibits a high sensitivity, a low detection limit, fast response and recovery properties to ethanol and acetone. The sensitivities of the RuO_2 modified petal-like ZnO based sensor to 100×10^{-6} ethanol and acetone at 360 °C are 33 and 67, respectively. The response and recovery times of the sensor are 4 s and 9 s to 10×10^{-6} ethanol, and are 3 s and 10 s to 10×10^{-6} acetone, respectively.

Key words: ZnO; RuO_2; nanosheets; gas sensing; ethanol; acetone

1 Introduction

Zinc oxide (ZnO), a functional n-type semiconductor with wide band gap (E_g ~3.7 eV) and large exciton binding energy (60 meV), has attracted great research interests for its unique optical and electrical properties in application of piezoelectric nanogenerators [1], solar cells, nanolasers [2], gas sensors [3,4], photocatalysis [5] and so on. The properties and performance of ZnO are closely dependent on its size, morphology and structures, therefore, more efforts have been devoted to synthesizing and preparing various ZnO nanostructures, such as nanowires [6], nanorods [7], nanobelts [8] and nanotubes [9,10]. The gas sensing properties and applications of the above ZnO nanostructures have been extensively concerned [11,12]. Recently, two-dimensional (2D) oxide nanosheets combining unique sheet-like morphology and porous structure have attracted significant research interests for their significantly enhanced properties in photoluminescence [13] and gas sensor applications [14]. SnO_2 nanosheets were synthesized by a hydrothermal method at 200 °C using stannic chloride hydrate and sodium hydroxide as starting materials. The response and recovery times of the SnO_2 sensor were 1 s and 9 s to 20×10^{-6} ethanol [15]. ZnO nanosheets were fabricated by an oxygen-assisted carbothermal reduction process and their properties were evaluated [16]. Using tris(hydroxymethyl)aminomethane as structure-directing agent, hexagonal ZnO nanosheets were also synthesized at approximately neutral pH (7.3), and the products showed a strong fluorescence at 590 nm [17]. ZnO nanosheets with intense green emission were synthesized at low temperature of 80 °C by a substrate-free, single-step, wet-chemical method [18]. Mn doped ZnO nanosheets were prepared by a microwave assisted chemical method, and their magnetic, optical and structural properties were investigated [19]. Porous and single-crystalline ZnO nanosheets were synthesized by annealing hydrozincite $Zn_5(CO_3)_2(OH)_6$ nanoplates, and they exhibited high selectivity and quick response to detecting acetone. Ru catalysts supported on ZnO by different Ru contents were prepared by an impregnation method and were applied to the vapor-phase selective hydrogenation of crotonaldehyde

Foundation item: Projects (61079010) supported by the National Natural Science Foundation of China and the Civil Aviation Administration of China; Project (3122013P001) supported by the Significant Pre-research Funds of Civil Aviation University of China; Project (2014) supported by the Science and Technology Innovation Guide Funds of Civil Aviation Administration of China

Corresponding author: Yan LI; Tel/Fax: +86-22-24092624; E-mail: liyan01898@163.com

DOI: 10.1016/S1003-6326(14)63424-5

[20]. ZnO nanorods were modified with $Ru(dcbpy)_2(NCS)_2$ (RuN_3), and their sensitivity to formaldehyde was higher than that of bare ZnO [21]. So far, RuO_2 modified ZnO nanosheets and their sensing properties are still rarely reported. However, the exploration of high sensitivity, rapid response and recovery characteristics of ZnO nanostructure is still a challenge.

We previously synthesized ZnO nanostructure in sheet or petal-like shapes [22]. In this work, we report the preparation and gas-sensing properties of petal-like ZnO nanosheets (ZS) and RuO_2 modified petal-like ZnO nanosheets (RZS) by a solvothermal method and calcination route, respectively. Excellent gas-sensing properties such as high sensitivity, quick response and recovery based on our sensor have been observed at 360 °C. In particular, the RZS based sensor shows low detection limit (1×10^{-6}), high sensitivity (33×10^{-6} ethanol and 67×10^{-6} acetone) and rapid response (4 s) and recovery (10 s) towards ethanol and acetone. The results demonstrate a promising approach to fabricate high performance ethanol and acetone sensors with high sensitivity, rapid response and recovery times.

2 Experimental

2.1 Preparation and characterization of ZnO nanosheets

In synthesis of petal-like ZnO nanosheets (ZS), all chemical reagents purchased from commercial market were of analytic grade and were used without further purification. Petal-like ZnO nanosheets were synthesized referring to our previous work [23], and the experimental conditions and routes were revised and optimized. Here, 0.1 mol/L $Zn(NO_3)_2{\cdot}6H_2O$ and 0.2 mol/L NaOH were prepared with 6 g $Zn(NO_3)_2{\cdot}6H_2O$, 1.2 g NaOH and deionized water, respectively. Then, the NaOH solution was slowly added into the $Zn(NO_3)_2{\cdot}6H_2O$ solution at room temperature under vigorous stirring to form a white suspension. The suspension was then separated with a centrifuge and washed three times with distilled water to obtain a white precipitate. The above precipitates were completely dispersed into an aqueous solution prepared with 0.01 g $C_{19}H_{42}BrN$, 10 mL ammonia and 45 mL ethanol, and the mixture was then sealed into a Teflon-lined autoclave with a filling capacity of about 60% and heated to 180 °C for 2 h. The resulting white precipitate was collected and washed with distilled water and absolute ethanol several times to obtain ZnO nanosheets.

In preparation of petal-like RuO_2−ZnO nanosheets (RZS), for RuO_2 deposition, 2 g of petal-like ZnO powders was dispersed in 3.3 mL ethanol, and then 80 mg, 120 mg and 160 mg of $RuCl_3$ (Ru 37% in mass fraction) were added in the above mixture respectively to prepare a series samples. After grinding in an agate mortar for about 30 min until the salts were dissolved and uniformly dispersed, the mixture was dried in the air and then placed into the muffle, which was heated to 400 °C (heating rate of 5 °C /min), and calcined for 2 h.

The products were characterized by a 1530VP model field emission scanning electron microscope (FESEM), and X-ray diffraction (XRD) with Cu K_α radiation (λ=0.1542 nm) on a DX−2000 X-ray diffractometer. Pacific BET surface area of ZnO nanosheets was measured using a Quantachrome 2010 model Autosorb station (US). RuO_2 content was calculated according to the dosage of $RuCl_3$ and confirmed by an energy dispersive spectrometer (EDS).

2.2 Fabrication and measurement of gas-sensing properties

The products were mixed with deionized water at a mass ratio of 4:1 to form a paste. The sensors were made with a coating ceramic tube with the paste to form a thin 10 μm sensing film. A pair of gold electrodes was installed at each end of the ceramic tube before it was coated with the paste; each electrode was connected with two Pt wires. A Ni−Cr heating wire was inserted into the tube to form an indirect-heated gas sensor. The structure of the sensor is shown in Fig. 1.

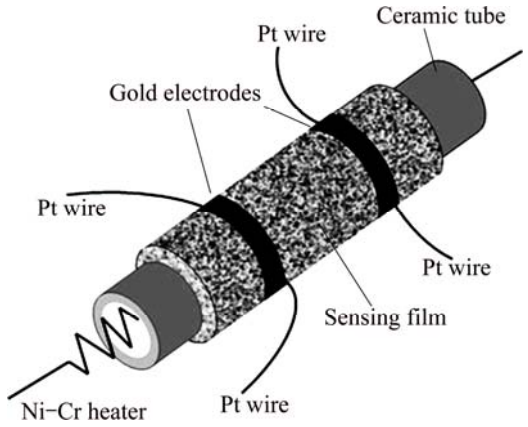

Fig. 1 Sketch of gas-sensor

The gas-sensing properties of the sensor were measured by a chemical gas sensor (8 Intelligent Gas Sensing Analysis System, China). The sensitivity (S) of the sensor was defined as the ratio of sensor resistance in dry air (R_a) to that in a target gas (R_g), which is expressed in Eq. (1):

$S=R_a/R_g$ (for reducing gas)

or

$$S=R_g/R_a \text{ (for oxidizing gas)} \quad (1)$$

where R_a and R_g are the sensor resistances in the air and testing gas environment, respectively.

The time taken by the sensor to achieve 90% of the total resistance change was defined as the response time in the case of adsorption and the recovery time in the case of desorption.

3 Results and discussion

3.1 Structure and morphology of ZnO nanosheets

Figure 2 shows the X-ray diffraction (XRD) patterns of the ZS and RZS. The products have a wurtzite structure and the diffraction peaks can be well indexed to hexagonal ZnO (JCPDS Card No.36−1451). The intense peaks of the XRD pattern indicated that the products were well crystallized. In addition, for ZS, no additional peaks were investigated by XRD, indicating the high purity of the ZnO products. The fine differences on the diffraction pattern between the ZS and the RZS are shown in the partial enlargement inserts in Fig. 2. Four additional minute diffraction peaks at 28.2°, 35.3°, 40° and 54.8° can be observed in the insert in Fig. 2(b) respectively, compared with the insert in Fig. 2(a), which can well match the characteristic peaks of RuO_2 (JCPDS Card No.21−1172). It is proven that $RuCl_3$ completely transformed into RuO_2 after calcination at 400 °C for 2 h.

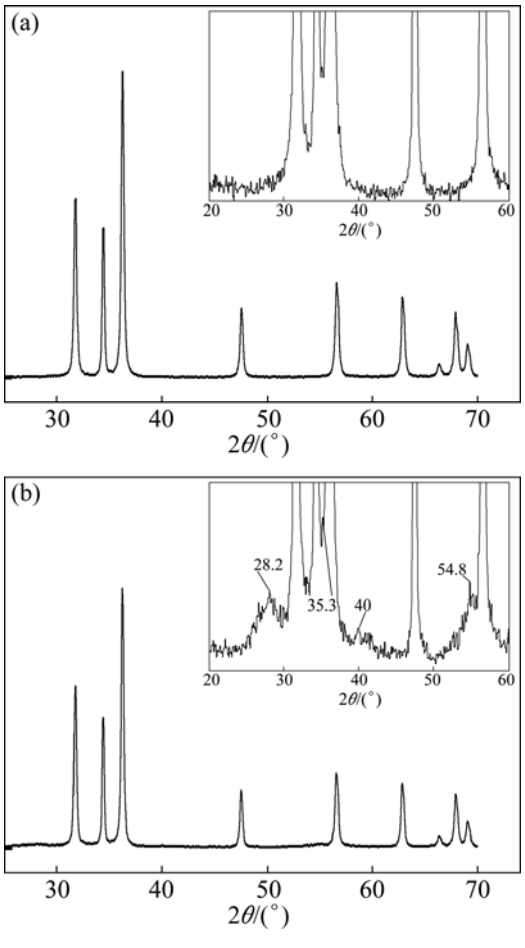

Fig. 2 XRD patterns of ZS (a) and RZS (b)

Figure 3(a) and (b) show the morphology of the as-synthesized ZnO nanosheets. Numerous flower-like and petal-like ZnO sheets can be clearly observed. The dimension of petals or sheets was 400 nm to 1 μm in diameter, and was 20 nm to 40 nm in thickness. It can be found that many petals clustered round to form a honeycomb or fishbone shaped structure. It can be predicted that the densification process can be avoided by the loose structure of flower-like ZnO during sensor preparation and ageing, by which the spread speed and diffusion speed of target gas are guaranteed for gas sensing uses. Figure 3(c) shows the rough surface of the RZS compared with ZS in Fig. 3(b). The different morphology mainly formed by absorbing RuO_2 nano particles onto the ZnO nanosheets. Ru content of 2.41% in the RZS was confirmed by EDS (see Fig. 3(d)).

The curves of N_2 adsorption−desorption isotherm of the ZS and the RZS in Fig. 4 exhibit a step increase in the volume of adsorbed nitrogen at a relative pressure of about 0.90, and the hysteresis in the high relative pressure range of (0.88−0.98)P/P_0, which belong to type IV. The calculation results revealed that the specific BET areas of the ZS and the RZS are 13.011 and 13.198 m^2/g respectively. This shows that the BET area of the ZS has not been changed by Ru-modification procedure. The relatively high surface area was due to the shape characteristics, which had a large size in two dimensions and a very small size in another dimension.

3.2 Gas-sensing properties

The working temperature range is a major functional characteristic for semiconductor oxide sensors. The sensitivity of sensors based on ZS and RZS nanoparticles to 20×10^{-6} ethanol and acetone as a function of operating temperature are displayed in Fig. 5. It can be observed that the sensitivity amplitude of the sensor exhibits peak-shaped depending on the operating temperature. It can be seen from the figure that, with increasing the operating temperature from 270 to 480 °C, the sensitivity of the ZS sensor increases slowly and reaches the maximum (5.26 to ethanol, 6.29 to acetone) at the operating temperature of 390 °C, and then decreases with further increasing the temperature. The sensitivity of the ZS sensor to acetone is higher than that to ethanol at the operating temperature. The similar results of the RZS sensor to ethanol and acetone can also be seen in Fig. 5. However, it is notable that the sensitivity of the RZS sensor to ethanol and acetone has a quick increasing speed compared with the ZS sensor in whole operating temperature range. In particular, the sensitivities of the RZS sensor to ethanol and acetone are significantly higher than those of the ZS sensor; the sensitivity of the RZS sensor to acetone is obviously higher than to ethanol. The maximum sensitivity of

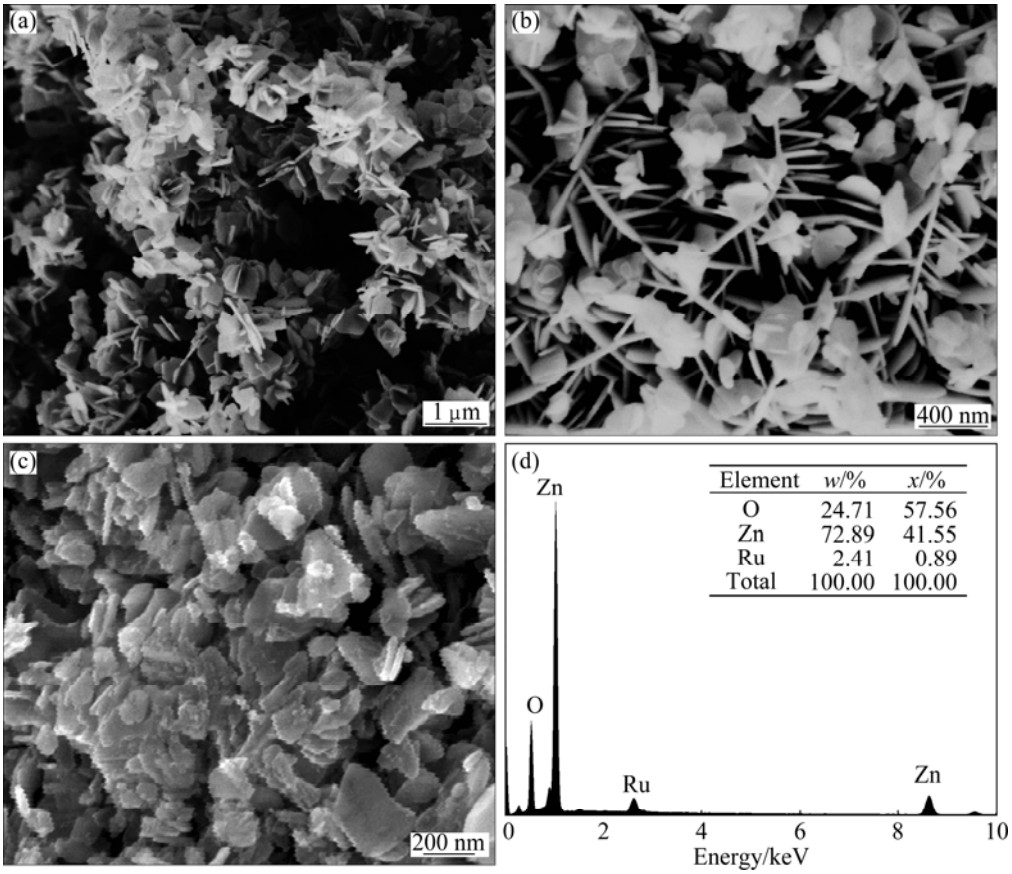

Fig. 3 FE-SEM images of ZS (a, b) and RZS (c) and EDS spectrum of surface of RZS (d)

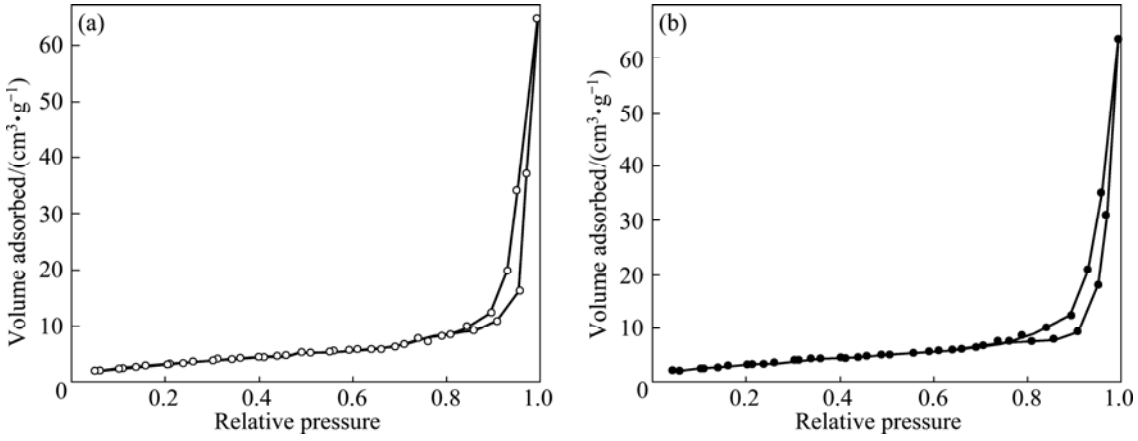

Fig. 4 Curves of N_2 adsorption−desorption isotherm of RZS (a) and ZS (b)

the RZS sensor to acetone appears at 360 °C, which is about 30 °C less than that of the ZS sensor to acetone and ethanol. The highest sensitivities of the RZS sensor to 20×10^{-6} ethanol and acetone were 8.9 and 13.4 respectively. It can be evaluated from Fig. 5 that, the sensitivities of the RZS sensor to ethanol and acetone are 2 times higher than those of the ZS sensor.

The dynamic sensing characteristics of the ZS and RZS based sensors to ethanol and acetone were examined, respectively. With the increasing test gas concentration from 1×10^{-6} to 100×10^{-6}, the sensitivities of the gas sensor are obviously improved. Figure 6(a) shows the sensitivities of the ZS sensor to 1×10^{-6}, 5×10^{-6}, 10×10^{-6}, 20×10^{-6}, 50×10^{-6} and 100×10^{-6} ethanol were 2.2, 2.7, 3.7, 5.5, 7.3 and 9.8, respectively. The response and recovery times of the sensor to 10×10^{-6} ethanol are 4 s and 5 s. Fig. 6(b) shows the sensitivities of the ZS sensor to 1×10^{-6}, 5×10^{-6}, 10×10^{-6}, 20×10^{-6}, 50×10^{-6} and 100×10^{-6} acetone are 1.6, 3.0, 4.5, 7.3, 8.7 and 13.4, respectively. The response and recovery times of the sensor to 10×10^{-6} ethanol are 2 s and 20 s. It is can be seen in Fig. 6(c) and (d) that, the sensitivities of the RZS

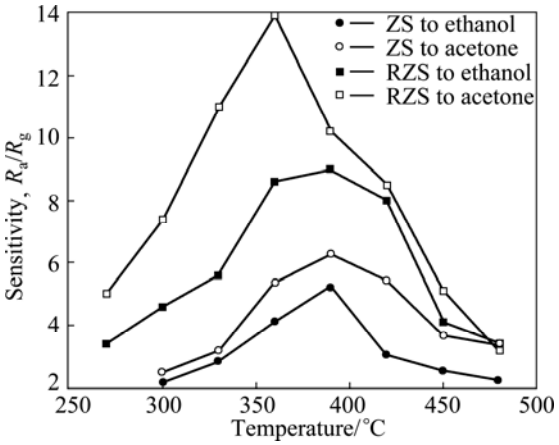

Fig. 5 Sensitivity of sensors based on ZS and RZS nanoparticles to 20×10^{-6} ethanol and acetone

sensor to 1×10^{-6}, 5×10^{-6}, 10×10^{-6}, 20×10^{-6}, 50×10^{-6} and 100×10^{-6} ethanol are 2.6, 5.1, 7.2, 9.6, 21.5 and 33.2, respectively, and the response and recovery times of the sensor to 10×10^{-6} ethanol are 4 s and 9 s; the sensitivities of the RZS sensor to 1×10^{-6}, 5×10^{-6}, 10×10^{-6}, 20×10^{-6}, 50×10^{-6} and 100×10^{-6} acetone are 2.6, 5.3, 7.7, 12.8, 32.4 and 67.6, respectively, and the response and recovery times of the sensor to 10×10^{-6} ethanol are 3 s and 10 s. Compared with the above series data from Fig. 5, it can be found that the sensitivities of the RZS sensor are dramatically higher than those of the ZS sensor to ethanol and acetone gas from 1×10^{-6} to 100×10^{-6}, especially in the high concentration range from 20×10^{-6} to 100×10^{-6}. The sensitivities of the RZS sensor are 3.4 and 5 times more than those of the ZS sensor to 100×10^{-6} ethanol and acetone, respectively. This quality is potentially useful for an improvement of gas sensor selectivity. The possible reason is attributed to the RuO_2 decorating, which efficiently activates the dissociation of molecular oxygen at different temperatures.

The linear functional relation between the sensing sensitivity and the gas concentration of the sensors to ethanol and acetone were plotted in linear fitting style in Fig. 7. It is revealed that the sensitivities of the RZS sensor dramatically increase with increasing gas concentration in the range from 1×10^{-6} to 100×10^{-6}, which is more than that of ZS sensor. The linear fitting equations are shown in Eq. (2) to Eq. (5):

RZS to acetone: S=1.08+0.65c, R=0.99 (2)

RZS to ethanol: S=3.85+0.30c, R=0.98 (3)

ZS to acetone: S=3.04+0.11c, R=0.90 (4)

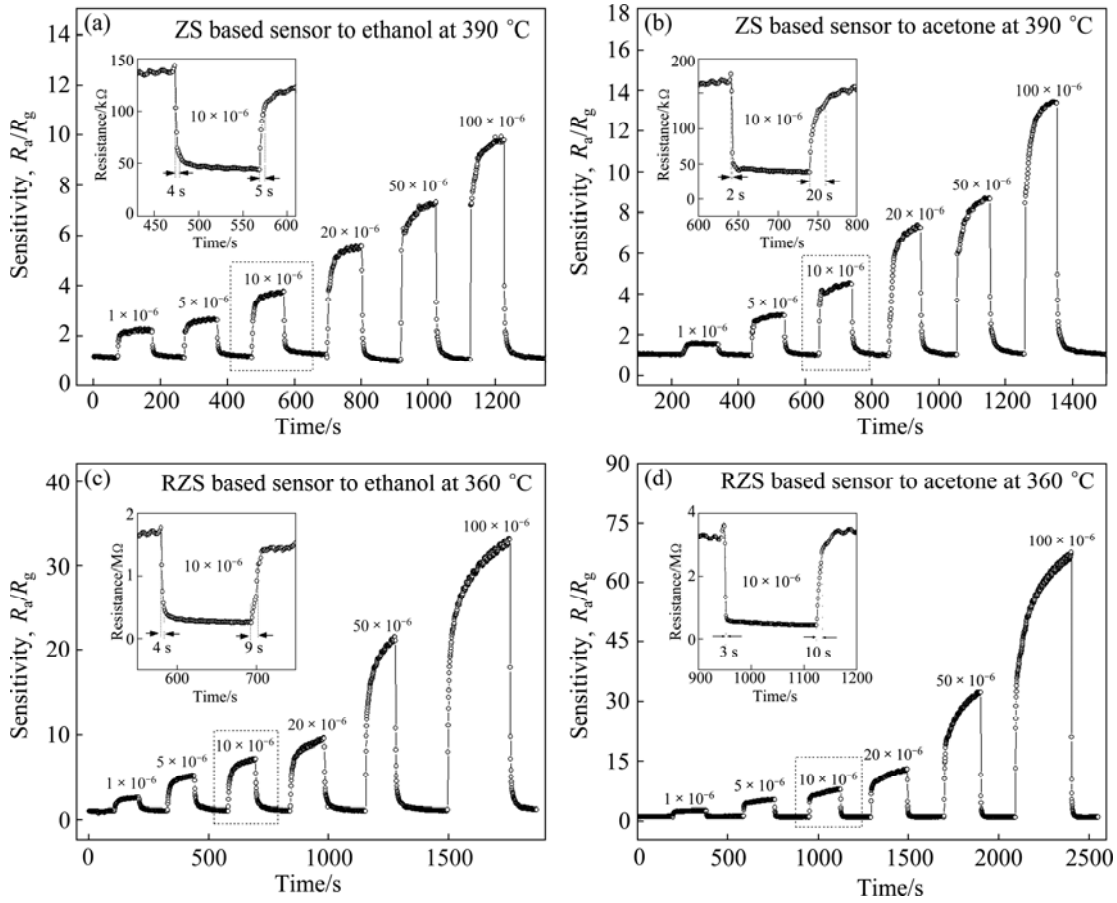

Fig. 6 Typical response and recovery characteristic curves of ZS sensor to ethanol (a) and acetone (b) in range of 1×10^{-6}–100×10^{-6} at 390 °C and RZS sensor to ethanol (c) and acetone (d) in range of 1×10^{-6}–100×10^{-6} at 360 °C

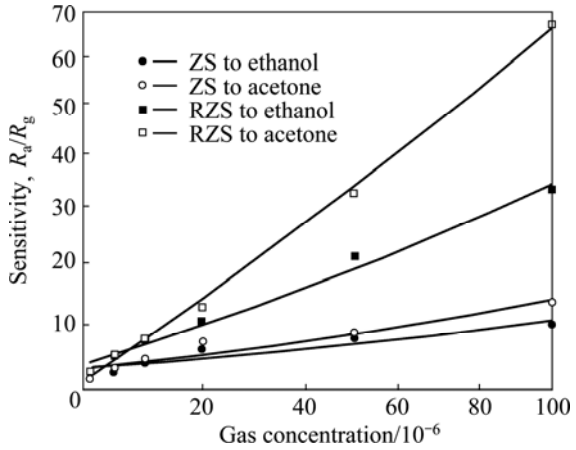

Fig. 7 Linear dependence of sensitivity on concentrations of ethanol and acetone in range of 1×10^{-6}–100×10^{-6}

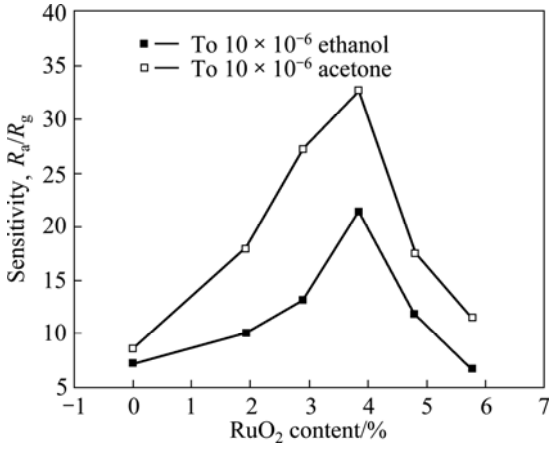

Fig. 8 Sensitivity of RZS sensor versus RuO_2 content calculated from $RuCl_3$ modified into ZS

ZS to ethanol: S=3.13+0.07c, R=0.87 (5)

where S is sensing sensitivity, c is the target gas concentration and R is the correlation coefficients.

The curve slope related to ZS sensors is very diminutive compared with RZS sensors. The correlation coefficients of the ZS sensor to ethanol, and acetone in the range from 1×10^{-6} to 100×10^{-6} are 0.87 and 0.90, respectively; The correlation coefficients of the RZS sensor to ethanol, and acetone in the range from 1×10^{-6} to 100×10^{-6} are 0.99 and 0.98, respectively. Furthermore, it can be found that the linear relation of the RZS sensor to ethanol and acetone is more excellent than that of the ZS sensor. This indicates that the deviation of the dots plotted according to the experimental data from the fitting lines was negligible; moreover, the sensitivity and linear relation of the sensors were greatly improved by RuO_2 modification.

The influence of RuO_2 modification on the gas sensing properties of petal-like ZnO is diagrammed in Fig. 8. With increasing the RuO_2 content, the sensitivities of the RZS sensor to acetone and ethanol clearly increase and reach the maximum at about 4.0% of RuO_2 content, and then rapidly decrease. It can be observed that the sensitivity of the RZS sensor to acetone is obviously higher than that to ethanol. The sensitivity increment speed of the RZS sensor to acetone is quicker than that to ethanol, and the RZS sensor is more suitable to acetone than ethanol. The selectivity of the RZS sensor between ethanol and acetone can be remarkably improved by RuO_2 modification to ZnO nanosheets.

The repeated tests of the sensor to 20×10^{-6} ethanol and acetone at 360 °C were carried out. Figure 9(a) shows that the sensitivity (13.5), response time (2−3 s) and recovery time (10−20 s) to 20×10^{-6} acetone at 360 °C kept an unchangeable value. The result was also observed in Fig. 9(b) to 20×10^{-6} ethanol gas, and the sensitivity, response time and recovery time to 20×10^{-6}

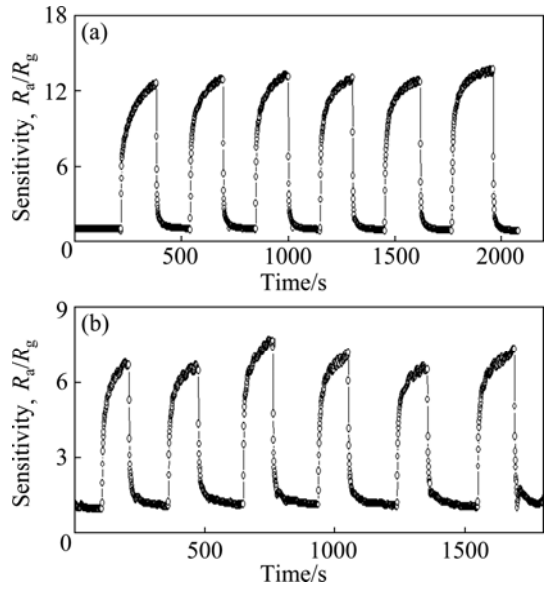

Fig. 9 Sensitivity of RZS sensor to 20×10^{-6} acetone (a) and ethanol (b) at 360 °C

ethanol at 360 °C were 9.5, 3−4 and 15−25 s, respectively. The sensitivity, response and recovery time were completely identical during six-loop testing. Moreover, the sensor was found to be stable during the experiment and we did not observe the saturation phenomenon when the gas concentration was 20×10^{-6}. It can be concluded that the RZS based sensor can be efficiently applied to detecting ethanol and acetone with various low concentrations.

The gas-sensing property of the RuO_2-modified ZnO nanosheets to acetone and ethanol is much better than that of petal-like ZnO nanosheets. This may be attributed to the incorporation of the interface between ZnO sheets and RuO_2 nanoparticles. As is known to all, noble metals are highly commended for catalyzing various reactions, such as hydrochlorination, low-temperature CO oxidation, and selective alcohol

oxidation, due to unique catalytic and electronic activities. For ZnO nanosheets, oxygen molecules can be adsorbed on the surface of the ZnO sample and form O^- or O^{2-}. Thus, a depletion layer on the ZnO rod surface is formed [24]. When the ZnO nanosheets are exposed to target gas, the molecules will react with the adsorbed oxygen species on the surface and release the trapped electrons back to the conduction band and lead to the increase of conductivity. However, by modification of RuO_2, oxygen molecules can be more easily adsorbed on the surface of ZnO nanosheets. This process increases both the quantity of adsorbed oxygen and the molecular conversion rate, resulting in the greater and faster degree of electron depletion from the ZnO nanosheets. Thus, the sensitivity of the RuO_2 modified ZnO nanosheets is distinctly higher than that of the unmodified ZnO nanosheets. On the other hand, different target gas supplies different number of free electrons to the sensor surface during sensor operating. Redox reaction formula of ethanol and acetone with O^- absorbed on the surface of sensors are shown in Eqs. (6) and (7):

$$C_2H_6O+6O^-=2CO_2+3H_2O+6e \quad (6)$$

$$C_3H_6O+8O^-=3CO_2+3H_2O+8e \quad (7)$$

According to Eqs. (6) and (7), the surface of sensing film traps more free electrons from C_3H_6O than C_2H_6O under a same concentration. It can be understood that the sensing response of RZS or ZS sensor to C_3H_6O is more sensitive than that to C_2H_6O in this gas sensing measurement. Though sensing response value is mainly determined by the surface area of sensor materials, target gas cannot effectively diffuse to contact whole surface due to a fact that most nanoparticles easily form various aggregates in use. In addition, although the surface area of the as-synthesized petal-like ZnO is lower than that of the reported products (75 m^2/g [25], 28.5 m^2/g [26]), the sensitivity, response and recovery speed to 10×10^{-6} ethanol and acetone were more excellent than those reported. For petal-like ZnO, the entire surface area remains exposed. Thus, high response and recovery speed were obtained. Gas diffusion length and gas diffusion speed are more important than the surface area of sensor materials in some cases, which affect the response and recovery times of semiconducting oxide gas sensors. The as-synthesized petal-like ZnO was made of numerous nanosheets, which heaped into a very loose honeycomb structure. Many tunnels were open to the sensing gas when the sensor materials were exposed to target gas, so the target gas can quickly diffuse to the surface of the sensor without any hamper.

4 Conclusions

1) Petal-like ZnO nanosheets and RuO_2 modified ZnO nanosheets synthesized by a solvothermal method and calcination route have a dimension of 400−1000 nm in diameter, and 20−40 nm in thickness. The BET surface area of the products is 13.198 m^2/g.

2) RuO_2 modified ZnO nanosheets based sensor exhibits excellent sensing performance, and the response and recovery times are 4 and 9 s to ethanol, 3 and 10 s to acetone at 360 °C, respectively. The minimal detection limits to ethanol and acetone are 1×10^{-6}. The maximum sensitivities of the RZS based sensor to 100×10^{-6} acetone and ethanol are 67 and 33, respectively.

3) The as-prepared RuO_2 modified ZnO nanosheets are potential candidate materials for high-performance gas sensors, which can be efficiently applied to detecting ethanol and acetone at a very low concentration.

References

[1] LEE J H, LEE K Y, KUMAR B, KIM S W. Synthesis of Ga-doped ZnO nanorods using an aqueous solution method for a piezoelectric nanogenerator [J]. Journal of Nanoscience and Nanotechnology, 2012, 12: 3430−3433.

[2] KIM A, WON Y, WOO K, KIM C H, MOON J. Highly transparent low resistance ZnO/Ag nanowire/ZnO composite electrode for thin film solar cells [J]. ACS Nano, 2013, 7: 1081−1091.

[3] SIMON Q, BARRECA D, GASPAROTTO A, MACCATO C, TONDELLO E, SADA C, COMINI E, SBERVEGLIERI G, BANERJEE M, XU K, DEVI A, FISCHER R A. CuO/ZnO nanocomposite gas sensors developed by a plasma-assisted route [J]. Chemphyschem, 2012, 13: 2342−2348.

[4] KIM K, LEE D H, JEONG D, DEBNATH P C, LEE D Y, KIM S, LEE S Y. Sensitivity-tuned CO gas sensors with tailored Ga-doping in ZnO nanowires [J]. Journal of Nanoscience and Nanotechnology, 2012, 12: 4211−4214.

[5] SADJADI S, ESKANDARI M. Ultrasonic assisted synthesis of imidazo[1,2-a]azine catalyzed by ZnO nanorods [J]. Ultrasonics Sonochemistry, 2013, 20: 640−643.

[6] MAHPEYKAR S M, KOOHSORKHI J, GHAFOORI-FARD H. Ultra-fast microwave-assisted hydrothermal synthesis of long vertically aligned ZnO nanowires for dye-sensitized solar cell application [J]. Nanotechnology, 2012, 23: 165602.

[7] RAI P, JO J N, WU X F, YOON J M, YU Y T. Synthesis of well dispersed, regular shape ZnO nanorods: effect of pH, time and temperature [J]. Journal of Nanoscience and Nanotechnology, 2011, 11: 647−651.

[8] WANG K, CHEN J, CHEN Y, ZHOU W. A large quantity synthesis of ultra-thin ZnO nanobelts induced from stacking faults [J]. Journal of Nanoscience and Nanotechnology, 2010, 10: 2257−2260.

[9] LI Y, LIU C S, ZOU Y L. Growth mechanism and characterization of ZnO nano-tubes synthesized using the hydrothermal-etching method [J]. Chemical Papers, 2009, 63: 698−703.

[10] LU H B, LI H, LIAO L, TIAN Y, SHUAI M, LI J C, FHU M, FU Q, ZHU B P. Low-temperature synthesis and photocatalytic properties of ZnO nanotubes by thermal oxidation of Zn nanowires [J]. Nanotechnology, 2008, 19: 045605.

[11] van HIEU N, KHOANG N D, TRUNG DO D, TOAN LE D, van DUY N, HOA N D. Comparative study on CO_2 and CO sensing performance of LaOCl-coated ZnO nanowires [J]. Journal of Hazardous Materials, 2013, 244−245: 209−216.

[12] LIU Y, ZHANG Y, LEI H, SONG J, CHEN H, LI B. Growth of

well-arrayed ZnO nanorods on thinned silica fiber and application for humidity sensing [J]. Optics Express, 2012, 20: 19404−19411.
[13] VEMPATI S, MITRA J, DAWSON P. One-step synthesis of ZnO nanosheets: A blue-white fluorophore [J]. Nanoscale Research Letters, 2012, 7: 470−479.
[14] XIAO Y, LU L, ZHANG A, ZHANG Y, SUN L, HUO L, LI F. Highly enhanced acetone sensing performances of porous and single crystalline ZnO nanosheets: High percentage of exposed (100) facets working together with surface modification with Pd nanoparticles [J]. ACS Applies Materials & Interfaces, 2012, 4: 3797−3804.
[15] LOU Z, WANG L L, WANG R, FEI T, ZHANG T. Synthesis and ethanol sensing properties of SnO_2 nanosheets via a simple hydrothermal route [J]. Solid State Electron, 2012, 76: 91−94.
[16] PARK J H, KANG G S, KWON S I, LIM D G, CHOI Y J, CHOI K J, PARK J G. Structural, optical, and electrical properties of semiconducting ZnO nanosheets [J]. Journal of Nanoscience and Nanotechnology, 2008, 8: 4658−4661.
[17] WANG H, JIANG H, ZHANG H, ZHOU Y, WU C, ZHAO J, WU C Y, BA L, WANG X M. One-pot synthesis of hexagonal ZnO nanosheets with a novel structure-directing agent and their application in cell imaging [J]. Journal of Nanoscience and Nanotechnology, 2011, 11: 1117−1122.
[18] PARK J Y, CHOI S W, KIM S S. A synthesis and sensing application of hollow ZnO nanofibers with uniform wall thicknesses grown using polymer templates [J]. Nanotechnology, 2010, 21: 475601.
[19] AHMED F, KUMAR S, ARSHI N, ANWAR M S, KIM G W, HEO S N, BYON E S, LEE S H, LYU N J, KOO B H. Magnetic, optical and structural property studies of Mn-doped ZnO nanosheets [J]. Journal of Nanoscience and Nanotechnology, 2012, 12: 5464−5468.
[20] LI B, HU G S, JIN L Y, HONG X, LU J Q, LUO M F. Characterizations of Ru/ZnO catalysts with different Ru contents for selective hydrogenation of crotonaldehyde [J]. Journal Industrial Engneering Chemistry, 2013, 19: 250−255.
[21] PENG L, QIN P, ZENG Q, SONG H, LEI M, MWANGI J J N, WANG D J, XIE T F. Improvement of formaldehyde sensitivity of ZnO nanorods by modifying with $Ru(dcbpy)_2(NCS)_2$ [J]. Sensors and Actuators B: Chemical, 2011, 160: 39−45.
[22] LI Yan, LIU Chuan-sheng. Hydro/solvo-thermal synthesis of ZnO crystallite with particular morphology [J]. Transactions of Nonferrous Metals Society of China, 2009, 19: 399−403.
[23] LI Yan, FENG Hui-yun, ZHANG Nan, LIU Chuan-sheng. Solvo-thermal synthesis and characterization of nest-like zinc oxide [J]. Transactions of Nonferrous Metals Society of China, 2010, 20: 119−122.
[24] LOU Z, DENG J, WANG L, WANG L, FEI T, ZHANG T. Toluene and ethanol sensing performances of pristine and PdO-decorated flower-like ZnO structures [J]. Sensor Actuators B, 2013, 176: 323−329.
[25] BURTON P D, PETERSON E J, BOYLE T J, DATYE A K. Synthesis of high surface area ZnO(0001) plates as novel oxide supports for heterogeneous catalysts [J]. Catalysis Letters, 2010, 139: 26−32.
[26] RAO J, YU A, SHAO C, ZHOU X. Construction of hollow and mesoporous ZnO microsphere: A facile synthesis and sensing property [J]. ACS Applies Materials & Interfaces, 2012, 4: 5346−5352.

花瓣状钌掺杂氧化锌纳米片的水热/煅烧法制备及气敏性能

李 酽，李国柱，邹云玲，王 琼，周青军，连晓雪

中国民航大学 理学院 航空化学研究所，天津 300300

摘 要：以硝酸锌、氢氧化钠为原料，通过水热/煅烧法制备结构新颖的厚度在 20 nm 至 40 nm 之间的钌掺杂花瓣状氧化锌纳米片。采用粉末 X 射线衍射仪、场发射扫描电镜、氮气吸附法、气敏测试系统对产物进行物相、结构形貌、比表面积、气敏性能等的表征。结果表明，钌掺杂氧化锌纳米片对乙醇和丙酮气体的灵敏度高，探测浓度低，响应和恢复迅速。在 360 ℃ 和 100×10^{-6} 的条件下，对乙醇和丙酮的灵敏度分别达到 33 和 67。在 10×10^{-6} 的乙醇和丙酮气体中，其响应和恢复速度分别为 4 s 和 9 s，3 s 和 10 s.

关键词：氧化锌；氧化钌；纳米片；气敏性；乙醇；丙酮

(Edited by Hua YANG)